

Chapter 3

Two-Photon transition

3.1 Introduction

One of the unique qualities of degenerate quantum systems is that all particles share the same phase. Although this phase is random between successively created condensates, the phase remains coherent over time for each production of a condensate [41, 58, 89, 90, 99, 102]. This is only true in the absence of external effects, such as thermal atoms and magnetic field variations. Investigation of phase properties requires the presence of another object which can interfere with the condensate in order to make the phase observable. The internal states of ^{87}Rb prove very useful, in that standard atomic physics magnetic-resonance techniques can be employed for interferometry. For experiments on trapped condensates the internal states used must have the same sign and magnitude of $\partial E/\partial B$ (the magnetic moment) in order that the states overlap spatially. Only the $|1, -1\rangle$ and $|2, 1\rangle$ states satisfy this. This chapter describes the two-photon transition first for a free atom in a uniform magnetic field, then for the complicated case of a confined atom in a time dependent magnetic field.

3.2 Transition for a free atom

The levels $|1, -1\rangle$ and $|2, 1\rangle$ (hereafter called $|1, -1\rangle$ and $|2, 1\rangle$ respectively) have the same magnetic moment to first order, and are separated by the hyperfine

splitting $\nu_{hs} \sim 6.8$ GHz. A two-photon drive is required since there are two units of angular momentum between them. Fig. 3.1 shows the $5S_{1/2}$ $F = 1$ and $F = 2$ ground states of ^{87}Rb in a small magnetic field which produces splittings of ~ 0.7 MHz/G between adjacent Zeeman levels. Also shown are the radio-frequency (~ 1 MHz) and microwave (~ 6.8 GHz) photons and their relative detunings. When the intermediate detuning is larger than the Rabi frequencies of the two level microwave and rf transitions ($\Omega_{-1 \rightarrow 0}^2$ and $\Omega_{0 \rightarrow 2}^2 \ll \Delta^2$) then the probability for a transition to the intermediate state $|2, 0\rangle$ is small. The three-level system can then be treated as a two-level system [68] with a Rabi frequency

$$\Omega_0 \equiv \frac{\Omega_{-1 \rightarrow 0} \Omega_{0 \rightarrow 2}}{2\Delta_{\text{IM}}}. \quad (3.1)$$

where all Ω are bare Rabi frequencies and Δ_{IM} is the detuning from the intermediate state. For arbitrary two-photon polarizations and Δ multiple paths must be considered to avoid interference or transitions to untrapped states. As an example, another possible arrangement is a microwave detuning below the $|2, 0\rangle$ state and increasing the rf energy. This opens up path to the $|2, -2\rangle$ state through the $|2, -1\rangle$ intermediate state if the required polarizations are present. Likewise, increasing the microwave frequency so that the intermediate state is higher in energy than the $|2, 1\rangle$, and changing the rf correspondingly, opens another path to the same final state $|2, 1\rangle$, but through the $|1, 0\rangle$, causing interference. The states $|2, 1\rangle$ and $|1, -1\rangle$ are sufficiently long lived that the linewidth is interaction time limited, meaning it is possible to measure the transition frequency to ~ 10 Hz. At this level the transitions have magnetic field dependence given by the Breit-Rabi formula

$$\nu(B) = -\frac{\nu_{hs}}{8} - g_I \frac{\mu_n}{h} B m_F \pm \frac{\nu_{hs}}{2} \sqrt{1 + m_F x(B) + x^2(B)} \quad (3.2)$$

$$x(B) = \left(g_J + \frac{g_I}{M_r}\right) \frac{\mu_b}{\nu_{hs} h} B \quad (3.3)$$

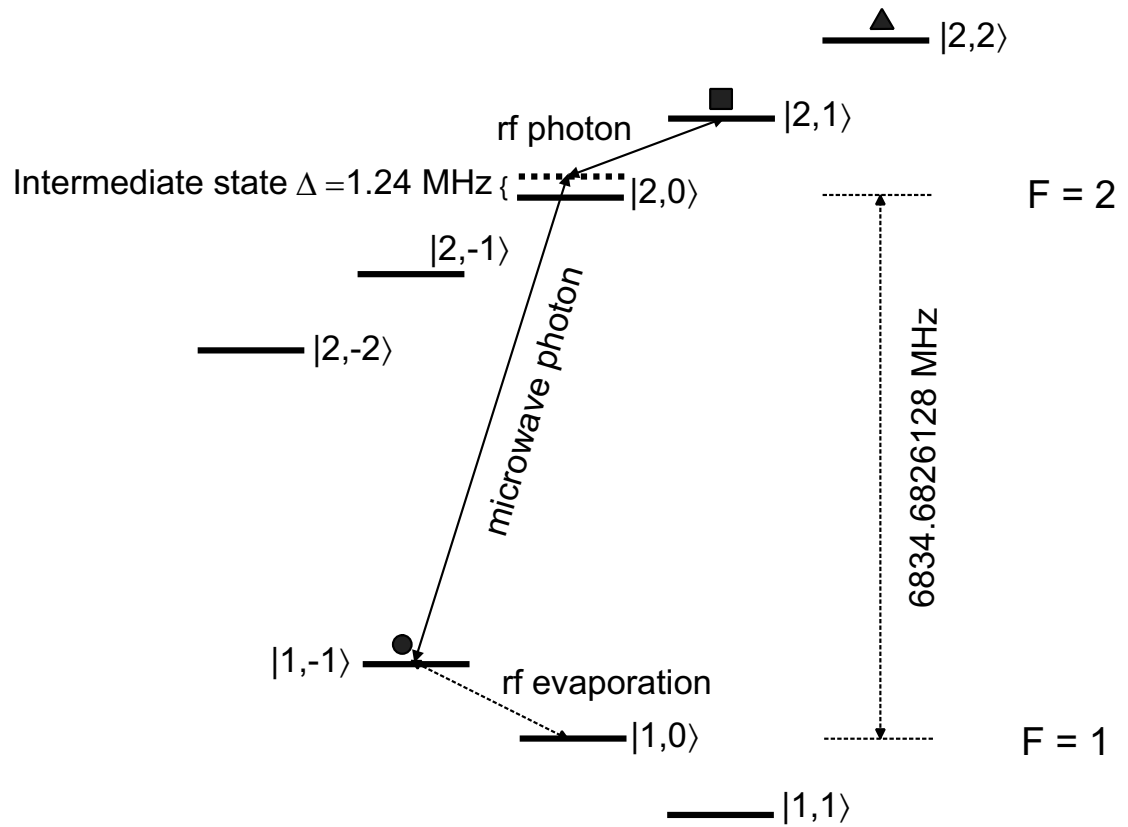


Figure 3.1: The ground states of ^{87}Rb in a small magnetic field. The states marked with squares have nearly the same magnetic moment. The state marked with the triangle is the only other trapped, but with twice the confinement of the other two. Microwave and rf photons couple the two states through an intermediate level.

$\frac{\mu_b}{h}$	1.399624 MHz/G
$\frac{\mu_n}{h}$	762.2591 Hz/G
$M_r = \frac{m_p}{m_e}$	1836.152701
g_I	$2.75124 \times \frac{2}{3}$
g_J	$2.002319 \times 1.0000059$
h	$6.6260755 \times 10^{-27}$ erg·s
ν_{hs}	6834.6826128 MHz [39]

Table 3.1: Useful constants

where the plus (minus) sign is used for $F = 2$ ($F = 1$) and the fundamental values in table 3.1 are useful [35]. This equation is exact for purposes here; the sphericity of the electronic orbit means that the field gradient at the nucleus is zero, giving no interaction with the nuclear charge distribution. All other interaction terms vanish by symmetry arguments, up to the small magnetic octupole moment [121].

Expansion of the function of $x(B)$ in Eq. 3.2 about small $x(B)$ is valid when the Zeeman splitting is small compared to the hyperfine splitting ($\mu_b B \ll h\nu_{hs}$), yielding the useful approximation for the frequency of any state

$$\begin{aligned} \nu(B) &= \left(-\frac{1}{8} \pm \frac{1}{2}\right)\nu_{hs} + \left(-g_I \frac{\mu_n}{h} \pm \frac{1}{4}\left(g_J + \frac{g_I}{M_r}\right)\frac{\mu_b}{h}\right)m_F B \\ &\pm \frac{1}{4\nu_{hs}}\left(1 - \frac{m_F}{4}\right)\left(\left(g_J + \frac{g_I}{M_r}\right)\frac{\mu_b}{h}B\right)^2. \end{aligned} \quad (3.4)$$

This evaluates to the simple expression for the transition frequency between $|1, -1\rangle$ and $|2, 1\rangle$, good to $< 1\text{Hz}$ up to $B = 20\text{G}$

$$\Delta\nu(B) = -2796.21B + 431.361B^2 + \nu_{hs}. \quad (3.5)$$

Eq. 3.5 is plotted in Fig. 3.2. The setup for driving the two-photon transition is shown in Fig. 3.3. Rf is applied through the same path as the evaporation rf; capacitively coupled onto the top quadrupole coil. Microwave is applied through a sawed-off waveguide of cross-section 2.2 cm by 1.0 cm, ~ 15 cm long, and ~ 3 cm from the center of the cell to the end of the guide. The cutoff frequency for the

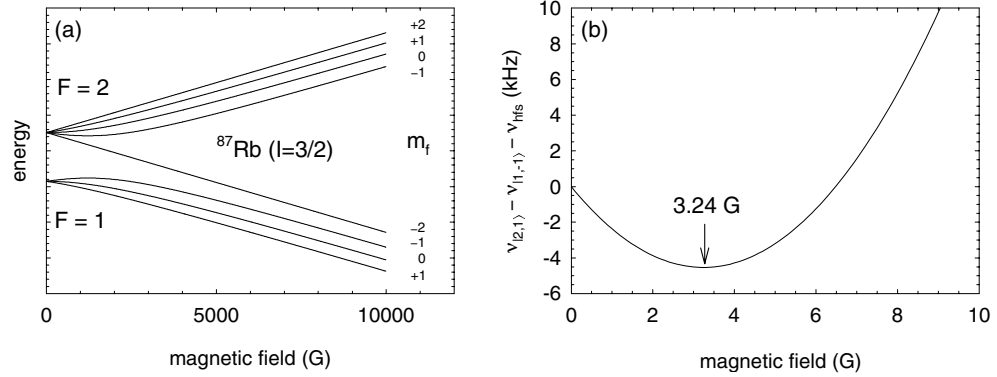


Figure 3.2: (a) The hyperfine and Zeeman levels as a function of bias field. The frequency splitting at $B=0$ is ν_{hs} . Figure (b) shows the energy difference between $|1, -1\rangle$ and $|2, 1\rangle$, where the energy difference at $B=0$ has been subtracted. At the special field value of $B = 3.24\text{G}$ the transition has no field dependence.

TE_{10} mode is 6.82 GHz ($\lambda = 4.4\text{ cm}$) [86]. Magnetic field polarization is along the long direction of the waveguide, or out of the page in Fig. 3.3, in the same direction as the rf. Since the quantization axis of a trapped atom is parallel to the page (rotating with the TOP field), this configuration provides equal amounts of $\sigma+$ and $\sigma-$ microwave and rf for all angles of the TOP field. Unfortunately, the presence of other conduction objects near the trap (coil supports, copper coils) distort the microwave field in an unknown way. Power is applied to the waveguide through rigid coax from a Hughes traveling-wave tube amplifier (20W), which is driven by an HP 8672A frequency source. Since our expected precision was ~ 1 part in 10^{10} , and we wanted the option of making absolute frequency measurements, the HP source was locked to an HP58503A GPS receiver with root Allen variance of $\sim 1 \times 10^{-12}$ over 1 second (10MHz signal). Before the amplifier input is a microwave switch for fast turn on. The amplifier output passes first through a high power directional coupler to prevent damaging reflections, then through a power splitter in reverse. The splitter takes power from the reflected wave to a square law detector for measuring the power on a scope.

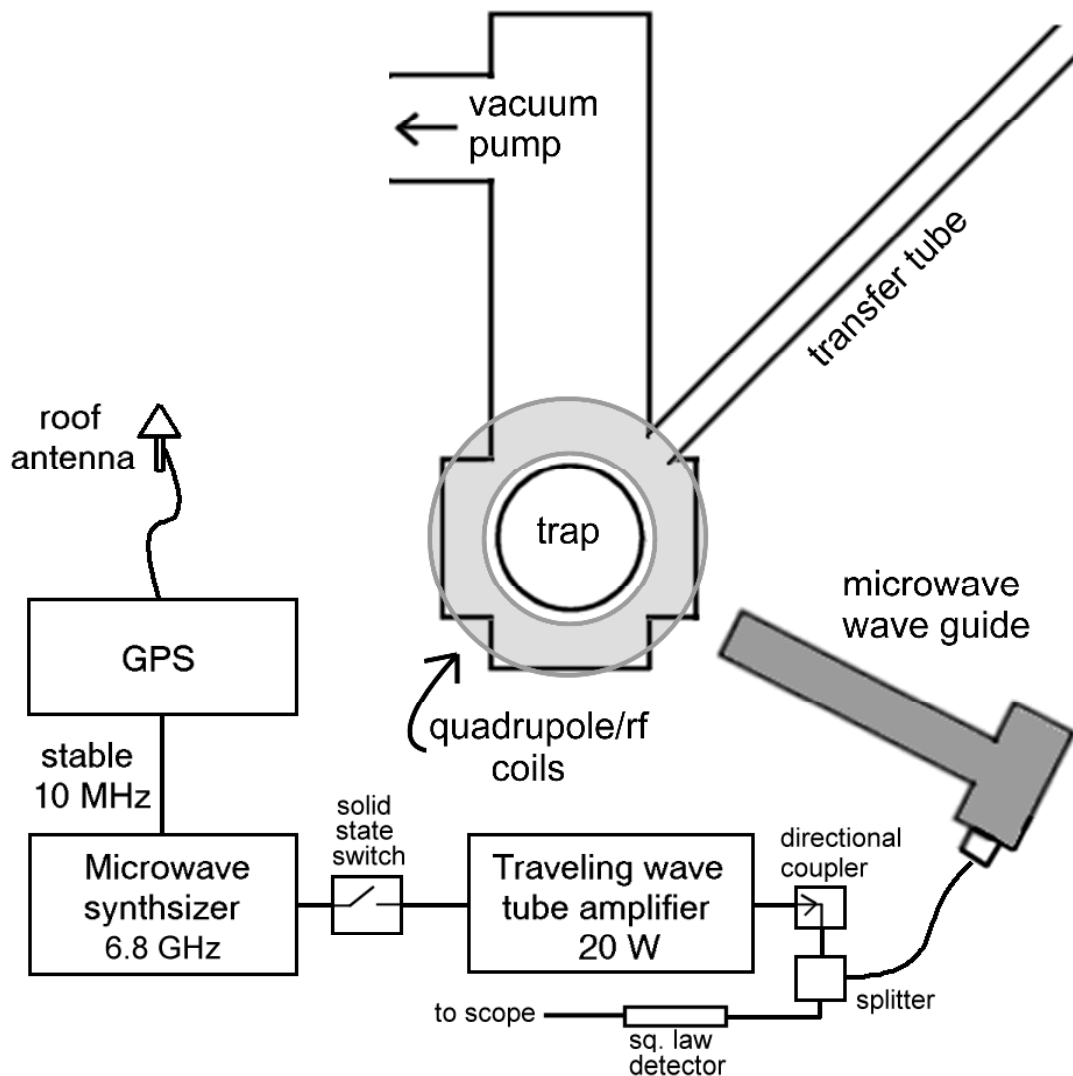


Figure 3.3: The position of the microwave waveguide is shown relative to the trap. Rf is capacitavly coupled to the top quadrupole coil (it is the same as the evaporation rf)

The rf is generated either by the rf synthesizer used for evaporation, or a separate synthesizer if the frequency switching time is not fast enough to go between evaporation and the two-photon drive. An rf switch is used to toggle between the two synthesizers. The remainder of the rf path is the same as for evaporation. Stability requirements for the rf are easily met by the devices without externally locking to the 10MHz GPS signal (although we do anyway).

For general superposition experiments, the rf and microwave pulses must be short compared to the trap frequency so that no density evolution occurs during the population transfer. Other experiments require arbitrary pulse sequences and timings. We use a programmable HP8672A for this task. Following is a description of the general timing for two-photon pulses. See [61] for details on condensate creation.

Programming of the HP8672A can easily require a few seconds of time given the 100 commands that must be uploaded for complex pulse sequences. This is done in two pieces; one after a command is changed from the experiment-computer keyboard, and the other once the experiment run has begun (after the atoms are transferred into the TOP trap). At this time the amplitude and frequency of various synthesizers is set, and the HP8176A is awaiting a trigger to begin its pulse sequence. Evaporation proceeds and a nearly pure condensate is created in the $F = 1, m_F = -1$ state. The trap can then be ramped to achieve the desired confinement. After things have settled (quadrupole coil temperature for example) a trigger from the computer is sent to the AF synchronization box, which outputs a trigger to the HP8176A only when the TOP field has a specific phase. This way all experiments are locked to the rotating TOP field, so that specific events will occur at the same field direction. This is critical for destructive, near-resonance imaging, obtaining a repeatable position of a dropped condensate, and keeping strange sideband behavior constant (see the Tilted TOP section in this chapter).

Fig. 3.4 shows a timing diagram for a simple separated oscillatory field experiment containing two two-photon pulses.

For initial experiments we drove single-photon microwave transitions from a dropped (B'_q turned to zero) condensate in the $|1, -1\rangle$ state to the $F = 2$ states. Initial linewidths were $\sim .3\text{MHz}$, making this a fair probe of magnetic field magnitude. This is interesting for calibration issues, especially one of rounding the rotating TOP field. Single-photon rf or microwave transitions means they are field sensitive at 0.7 MHz/G for rf drives, and multiples (up to 3) of $.7\text{ MHz/G}$ for microwave. Given that the linewidth is interaction time limited, and that the drive must be on for, at most, $1/4$ of a TOP rotation to sample only a given angle, means that the transition width is $4\nu_{TOP}$. This effectively detects a field difference of $\frac{4}{10}\nu_{TOP}/.7 \times 10^6\text{Hz}$ if the line can be split to 1 in 10. For a 7.2kHz rotation frequency this means an eccentricity of 4mG can be observed in the best case scenario.

The two-photon resonance from $|1, -1\rangle$ to $|2, 1\rangle$ was easily observed by applying both rf and microwave drives for a few milliseconds and observing the atoms in the $F = 2$ levels. Figure 3.5 shows typical data. Sidebands are a common feature in these lineshapes and are separated from the main peak by the TOP rotation frequency. An asymmetry is very common, with the right sideband larger than the left. This will be covered in more detail later.

Ramsey's method of separated oscillatory fields [121] was also employed for a host of frequency measurements in characterizing the system. Two common implementations are shown in Fig. 3.6 for dropped condensates. Graph 3.6(a) shows the signal as the time between two $\pi/2$ pulses of length $278\ \mu\text{s}$ is changed, and the two-photon drive is detuned by 850 Hz . The observed oscillation frequency is the difference between the atomic splitting and the drive. Essentially, this is a comparison of the rate of phase accumulation (energy) between the synthesizer

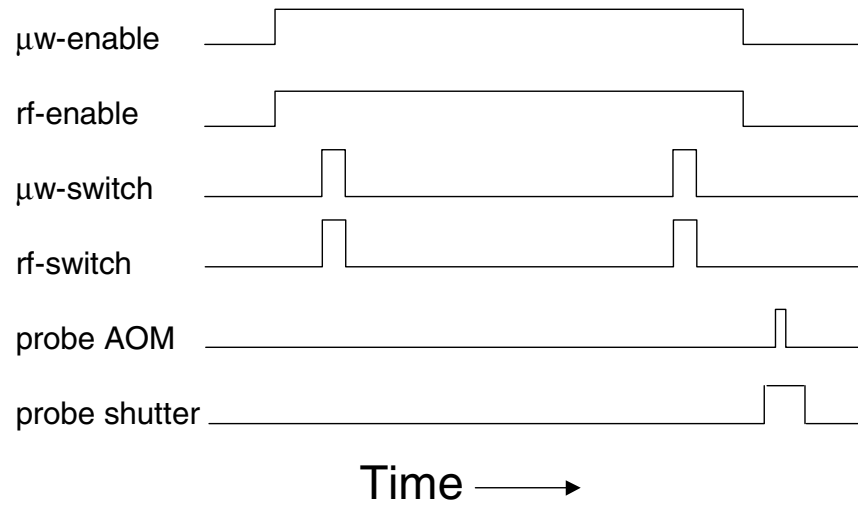


Figure 3.4: A basic timing diagram for a two-pulse experiment. The microwave and rf switch pulses can be any desired length, but are $\sim 1\text{ms}$ for most π -pulses.

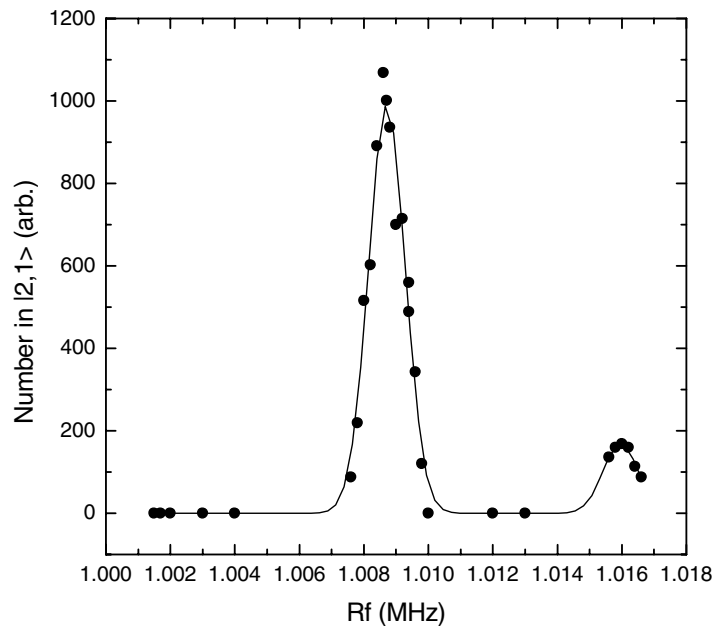


Figure 3.5: A typical Rabi lineshape for the two-photon resonance in a dropped condensate. The microwave is 6833.668 MHz, and the pulse is $690\mu\text{s}$ long. The sideband is separated by $\sim 7.2\text{ kHz}$, equal to the TOP rotation frequency.

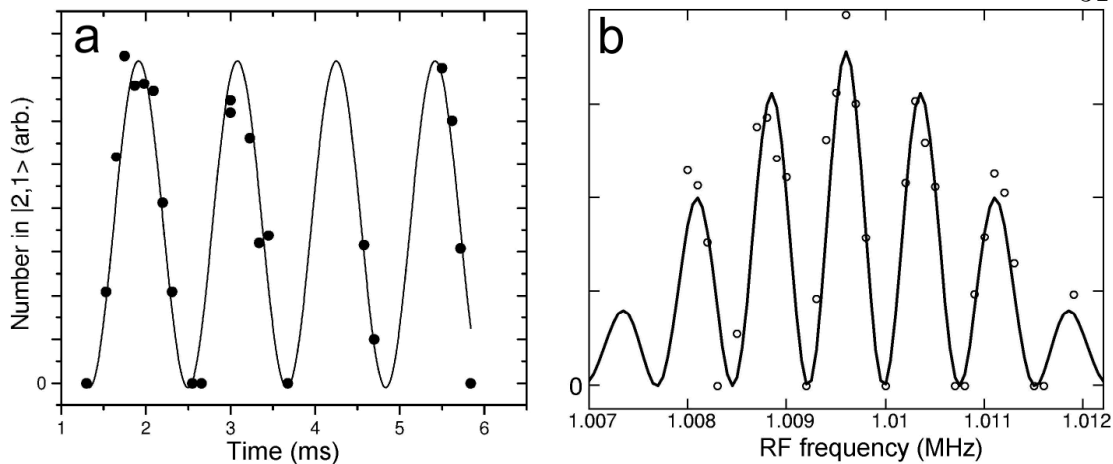


Figure 3.6: Ramsey’s method of separated oscillatory fields by changing the time between (a) or the frequency of (b) the two pulses. (a) The fit frequency gives the detuning between the drive and the atomic transition. (b) The solid line is a fit with adjustable amplitude and central frequency.

and the condensate, during the time between the pulses. The mean-field energy is the same for each point in this case; the system is in the same superposition of the two states for each data point. A more common case is shown in Fig. 3.6(b), in which the time between the pulses is constant at 1.02 ms, but the drive frequency changes. Since the superposition changes as a function of detuning, a systematic broadening could occur if the mean-field energy of the two states were unequal. The first case is used extensively in the following chapters as calibration of field amplitudes and in measuring phase properties of a condensate.

3.3 Transition for a trapped condensate

The preceding analysis is sufficient for a static magnetic trap. Additional complications arise, however, when a time-dependent magnetic trap (such as the TOP trap) is used to provide the confinement. Referred to as the “Weird Bohn Effect”, the time dependence leads to an additional effective static magnetic field which yields energy level shifts and vertical offsets between $|1, -1\rangle$ and $|2, 1\rangle$. It

has become a useful tool in double-condensate systems.

3.3.1 Quantum mechanical derivation

The TOP trap involves a magnetic field of magnitude B_0 rotating counterclockwise (as viewed from the positive z -axis) at angular frequency ω_t in the xy -plane,

$$\mathbf{B}_0(t) = B_0(\cos \omega_t t \hat{\mathbf{x}} + \sin \omega_t t \hat{\mathbf{y}}). \quad (3.6)$$

The effective Hamiltonian in a frame co-rotating with the magnetic field transforms as

$$\hat{H}_{\text{eff}} = R(-\omega_t t) \hat{H}_{\text{BR}} R^\dagger(-\omega_t t) - i \hbar R^\dagger(-\omega_t t) \frac{\partial}{\partial t} R(-\omega_t t) \quad (3.7)$$

with the time-dependent rotation operator R defined by

$$R(-\omega_t t) = \exp\left(\frac{i}{\hbar} F_z \omega_t t\right). \quad (3.8)$$

The operator F_z is the z -component of the total (nuclear plus electronic) spin vector, and the sign of the argument of R is chosen to rotate the coordinate axes in the same sense as the field. The Breit-Rabi Hamiltonian \hat{H}_{BR} (with eigenvalues Eq.3.2) is invariant under the transformation. We therefore obtain

$$\hat{H}_{\text{eff}} = \hat{H}_{\text{BR}} - F_z \omega_t. \quad (3.9)$$

The expectation value of this operator on a state $|F, m_F\rangle$ is

$$\begin{aligned} \langle F, m_F | \hat{H}_{\text{eff}} | F, m_F \rangle &= E_{\text{BR}} - \hbar m_F \omega_t = g_F m_F \mu_B B - \hbar m_F \omega_t \\ g_{F=1} &= -\frac{1}{4} g_J - \frac{5}{4 M_r} g_I \simeq -\frac{1}{2} \\ g_{F=2} &= \frac{1}{4} g_J - \frac{3}{4 M_r} g_I \simeq \frac{1}{2} \end{aligned}$$

where E_{BR} is written as only the largest part of Eq. 3.2, *i.e.* the first order Zeeman shift. Interpreting the expectation value of \hat{H}_{eff} as an effective magnetic

field $g_F m_F \mu_B B_{\text{eff}}$, we see that the rotating magnetic field becomes simply another static field contribution:

$$B_{\text{eff}} = B_0 - \frac{\omega_t \hbar}{\mu_B g_F} \quad (3.10)$$

3.3.2 Classical derivation

A classical derivation is more intuitive and yields the same result [121]. The equation of motion for a spin vector \mathbf{F} in a constant magnetic field \mathbf{B} is

$$\hbar \frac{d\mathbf{F}}{dt} = \mu_B g_F \mathbf{F} \times \mathbf{B}_0. \quad (3.11)$$

For magnetic field rotating at ω_t , the time derivative in the rotating frame becomes

$$\frac{d\mathbf{F}}{dt} = \vec{\omega}_t \times \mathbf{F} + \frac{\partial \mathbf{F}}{\partial t}. \quad (3.12)$$

Combining these two and solving for the motion of the vector in the rotating frame gives

$$\begin{aligned} \hbar \frac{\partial \mathbf{F}}{\partial t} &= \mu_B g_F \mathbf{F} \times \mathbf{B}_{\text{eff}} \\ \mathbf{B}_{\text{eff}} &= \mathbf{B}_0 + \mathbf{B}_\omega \\ \mathbf{B}_\omega &\equiv \frac{\hbar \vec{\omega}_t}{\mu_B g_F} \end{aligned} \quad (3.13)$$

which is the same as Eq. 3.10. This extra static field can be interpreted as an imaginary field which causes the spin vector to precess at a Larmor frequency ω_t . The magnitude of B_ω is only 2.6 mG for $\omega_t = 1.8\text{kHz}$, but switches sign for the two different hyperfine states. However since \mathbf{B}_ω is perpendicular to \mathbf{B}_0 , the total field magnitude remains constant in this picture. Only when another field with some component along \mathbf{B}_ω is present does this modify the actual magnitude, and hence two-photon transition energy. This is the case for an untrapped condensate,

as long as there is an external field along \mathbf{B}_ω . The total field is

$$|B_{\text{total}}| = \sqrt{B_0^2 + (B_z \pm B_\omega)^2} \quad (3.14)$$

where B_z is an external uniform field in the same direction as B_ω and the plus (minus) sign is used for the $|2, 1\rangle$ ($|1, -1\rangle$). The field for each state from Eq. 3.14 must be used in Eq. 3.4, and the difference taken to find the transition frequency. A useful approximation for the transition frequency is

$$\Delta\nu = -2796.21B_0 + 431.361B_0^2 + 699579\frac{B_\omega B_z}{B_0} \quad (3.15)$$

valid for $B_0 \gg B_\omega, B_z$. The first data investigating this effect was taken using condensates dropped from the trap, so that the magnetic gradient was off and only the rotating field B_0 and background field B_z present. Figure 3.7 shows this data and plots of the exact version of 3.15 for different directions of B_0 rotation (or equivalently, different signs of B_z). The extra term in Eq. 3.15 applies an offset whose magnitude drops off as B_0 dominates the total field.

The situation is similar for a trapped condensate, except that the confining gradient provides B_z . In the TOP trap gravity displaces the equilibrium position of the condensate from $z = 0$. The total instantaneous field at any point in the trap is

$$|B_{\text{total}}(z)| = \sqrt{(B_0 \cos(\omega t) + \frac{B'_q}{2}x)^2 \hat{\mathbf{x}} + (B_0 \sin(\omega t) + \frac{B'_q}{2}y)^2 \hat{\mathbf{y}} + (-B'_q z \pm B_\omega)^2 \hat{\mathbf{z}}}. \quad (3.16)$$

Figure 3.8 shows graphically the orientation of the fields in the TOP trap. The imaginary field B_ω points along $\vec{\omega}$. Since $z \neq 0$ when gravity is included the effect of B_ω is to modify the vertical quadrupole gradient with an offset. This can be rewritten as an offset in z , *i.e.* ,

$$\begin{aligned} (-B'_q z \pm B_\omega)^2 &= (-B'_q(z \pm z_\omega))^2 \\ z_\omega &\equiv \frac{B_\omega}{B'_q} \end{aligned}$$

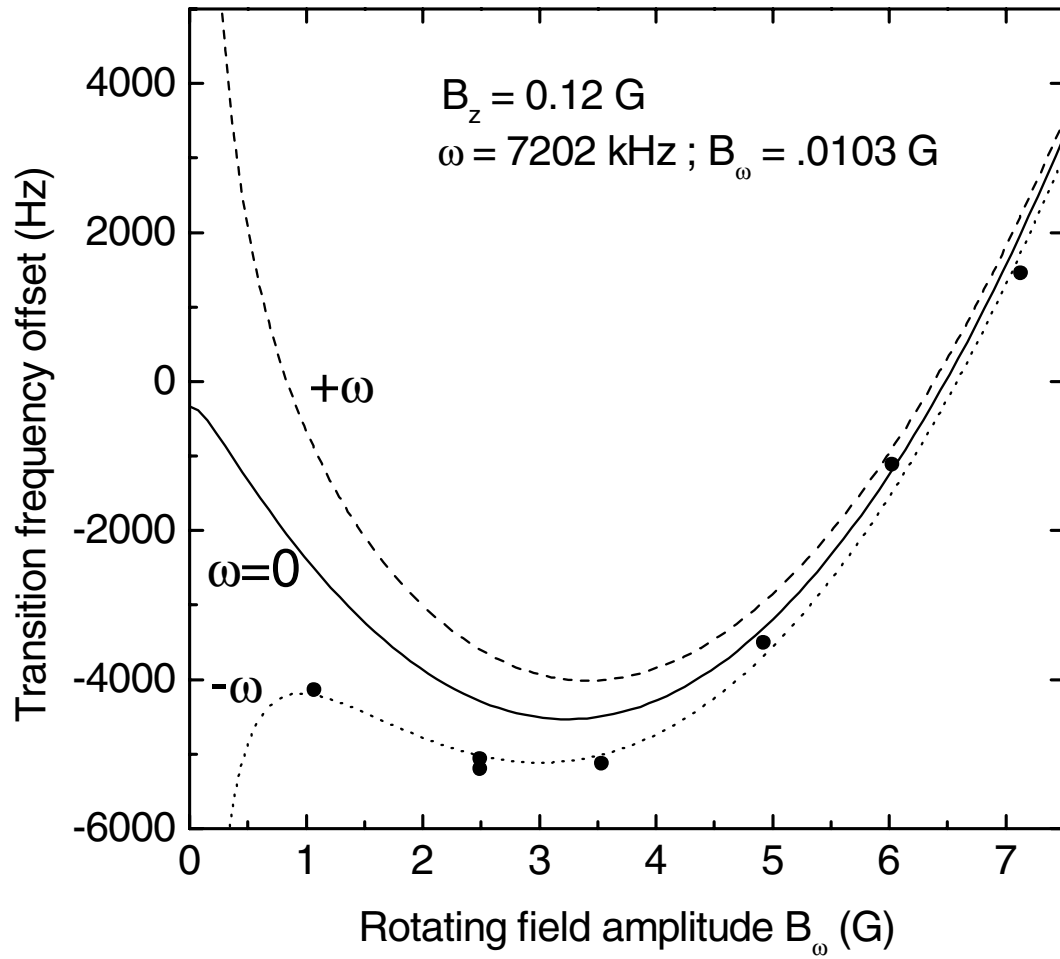


Figure 3.7: The data points are for a dropped condensate. The frequency of rotation of B_0 is 7.2 kHz and the vertical component of the background field B_z is found from a fit of Eq. 3.15. Also shown are the curves for the opposite rotation of B_0 and when there is no rotation.

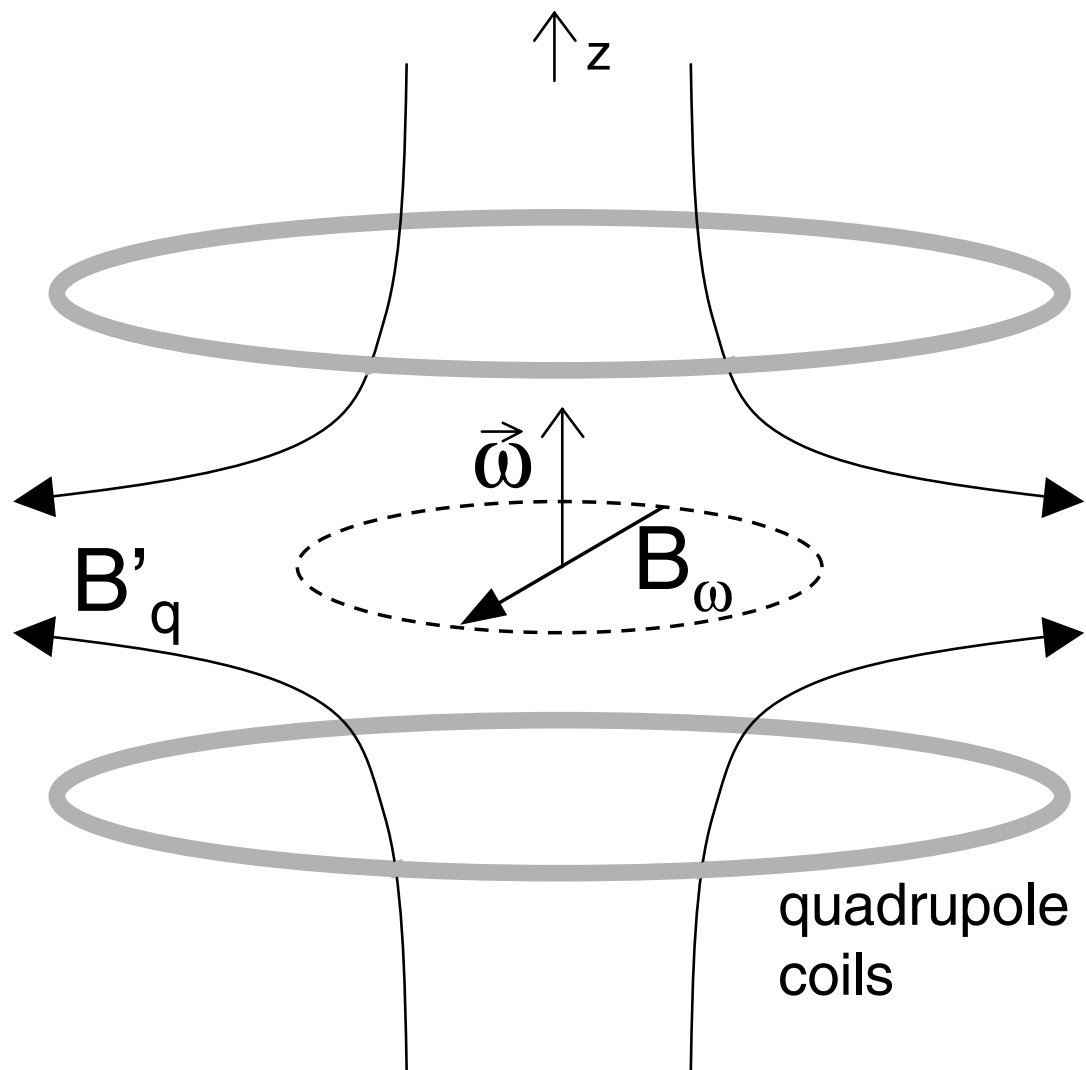


Figure 3.8: Diagram of the magnetic fields in a TOP trap. The curved arrows represent the field line from the quadrupole field B_q produced by the coils. A uniform field B_ω rotates about the central axis, providing an imaginary field B_ω along $\vec{\omega}$.

It is the total field in Eq. 3.16, along with the position $z \pm z_\omega$ of the atoms in the trap, which must be substituted into Eq. 3.2 to find two-photon transition frequency.

3.3.3 Observable effects

These equations can all be put together to yield useful quantities, such as the relative separation between the states and the transition frequency as a function of trap parameters. For the following quantities, the condensate is assumed to be at its equilibrium position, as defined by the trap parameters B_0, B'_q and B_ω . The following are small effects which are only observable for specific trap geometries, or when looking at differences in large quantities.

In general the position of an atom in a magnetic potential is found by setting the spatial derivative of the total energy to zero. From Eq. 3.2 and Eq. 3.16, the following must be solved for z ;

$$\frac{\partial}{\partial z} (h\nu(|B_{total}(z)|) + mgz) = 0.$$

This is a very complicated equation in z and not easily solved exactly. Using the expansion in Eq. 3.4 gives a quartic equation in the vertical position z whose solution is approximated by the expansion in ϵ

$$\begin{aligned} z = & \mp z_\omega + \frac{B_0}{B'_q} \frac{\eta}{\sqrt{1-\eta^2}} - 2 \frac{B_0^2}{B'_q} \frac{\eta}{(1-\eta^2)^2} \epsilon \\ & - 2 \frac{B_0^3}{B'_q} \frac{3\eta^2 + 2}{(1-\eta^2)^{\frac{7}{2}}} \epsilon^2 + 16 B_0^4 \frac{3\eta^3 + 2\eta}{(1-\eta^2)^4} \epsilon^3 \end{aligned} \quad (3.17)$$

in which $\eta \equiv \frac{mg}{KB'_q}$, $\epsilon \equiv L/K$, and K and L are the coefficients of the linear and quadratic Zeeman terms in Eq. 3.4 respectively. This reduces to Ensher's result (Eq. 6.9 [61]) when the nuclear and higher order Zeeman structure vanish ($\epsilon \rightarrow 0$ and $K \rightarrow \frac{1}{4} g_J \frac{\mu_B}{h}$). K, L and z_0 depend on the atomic state m_F . The size of the higher order terms is actually quite small compared to zero order. It is only when

looking at the difference in vertical position of the two states that these terms play significant role. As will be shown later these differences have quite a large effect in double condensate behavior.

Fig. 3.9 shows the effect of the trap rotation and the higher order magnetic field dependence on the relative vertical position of the two states. The effect of trap rotation is only to apply a vertical offset between the states in Fig. 3.9a. For many double-condensate experiments we are interested in traps where the relative offset is zero so that the condensates completely overlap. Fig. 3.9b is a plot of the rotating field magnitude B_0 necessary for overlap as a function of the quadrupole gradient B'_q . Only a very small range is accessible when the rotating field has a positive direction. Qualitatively the offset from rotation is opposing ($-B_\omega$ case) or enhancing ($+B_\omega$ case) the relative sag caused by the different higher order Zeeman shifts. All of the double-condensate experiments are done with the $-B_\omega$ rotation.

Using Eq. 3.17 for the position of atoms in the trap the absolute magnetic field, and hence the transition frequency, can be found as a function trap parameters. The total field at the equilibrium position of a state is given by the approximation

$$\begin{aligned}
 |B_{total}| &= \sqrt{B_0^2 + B_q'^2 z_0^2} - 2B_q' B_0 \frac{\eta \epsilon}{(1 - \eta^2)^2} \left(\frac{z_0}{\sqrt{B_0^2 + B_q'^2 z_0^2}} \right) \quad (3.18) \\
 &\simeq \frac{B_0}{\sqrt{1 - \eta^2}} \\
 z_0 &\equiv \frac{B_0}{B_q'} \frac{\eta}{\sqrt{1 - \eta^2}}
 \end{aligned}$$

where z_0 is the lowest order term in the vertical position from Eq. 3.17. This is independent of the rotating field frequency since its effect is to apply an offset in the vertical field which only moves the equilibrium position, but does not change the field the atoms experience. To calculate the transition frequency between

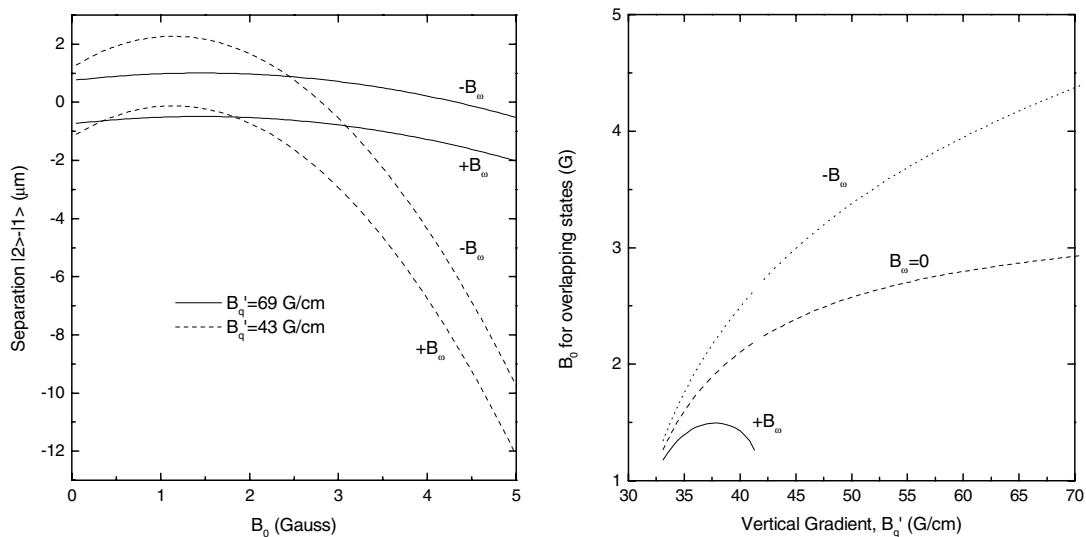


Figure 3.9: (a) The relative positions of the two states in the trap for two different values of the vertical gradient, with $\omega_t = 1800 \text{ kHz}$. In each pair of lines are the plots for different rotation directions of the TOP field. As $B_0 \rightarrow 0$ the lines for a particular gradient are separated by $2B_w/B'_q = 2z_0$. (b) The magnitude of B_0 necessary to have overlapping condensates as a function of B'_q , for the different rotation directions and without including the rotating effect.

$|1, -1\rangle$ and $|2, 1\rangle$, Eq. 3.18 must be used to calculate the field seen by each state. Since the atoms will be at the equilibrium position of the initial state ($|1, -1\rangle$ for instance), Eq. 3.18 is used with the appropriate η, z_0 and ϵ for $|1, -1\rangle$. The field B_2 experienced by $|2, 1\rangle$ is not only different through the terms η, z_0 and ϵ , but also because it is offset from its equilibrium position by an amount $2B_\omega/B'_q$, which must be added to z_0 in Eq. 3.18. The transition frequency of Eq. 3.5, minus the hyperfine splitting ν_{hs} , becomes

$$\Delta\nu = -g_I \frac{\mu_n}{h} (B_1 + B_2) + \frac{\mu_b}{4h} (g_J + \frac{g_I}{M_r}) (B_2 - B_1) + \frac{3}{16\nu_{hs}} \left((g_J + \frac{g_I}{M_r}) \frac{\mu_b}{h} \right)^2 (B_1^2 + B_2^2) \quad (3.19)$$

This is plotted in Fig. 3.10 as a function of the rotating field B_0 for two different values of B'_q . The effect of changing the direction of the rotating field is to offset the transition frequency. For many experiments we wish to operate in the region where the transition is insensitive to field noise (or rotating field asymmetries). This is the zero-slope point in Fig. 3.10, where the total field experienced by the atoms is 3.241 G. The rotating field magnitude required to reach this point is given by the approximation

$$\begin{aligned} B_0 &= \sqrt{1 - \eta^2(B'_q)} \left(\eta B_\omega + 3.241 \left(1 - \frac{1}{2}(1 - \eta^2) \frac{B_\omega^2}{3.241^2} \right) \right) \\ &\simeq 3.241 \sqrt{1 - \eta^2(B'_q)}. \end{aligned} \quad (3.20)$$

The second approximation is very good; it is nearly independent of B_ω (off by 10 mG for a factor of 10 change in the rotation frequency).

Unfortunately, the requirements for overlapping condensates is not the same as the requirement in Eq. 3.20. A contour plot of the slope of the transition ($\partial\Delta\nu/\partial B_0$) is shown in Fig. 3.11 along with the trajectory for overlapping condensates from Fig.3.9b.

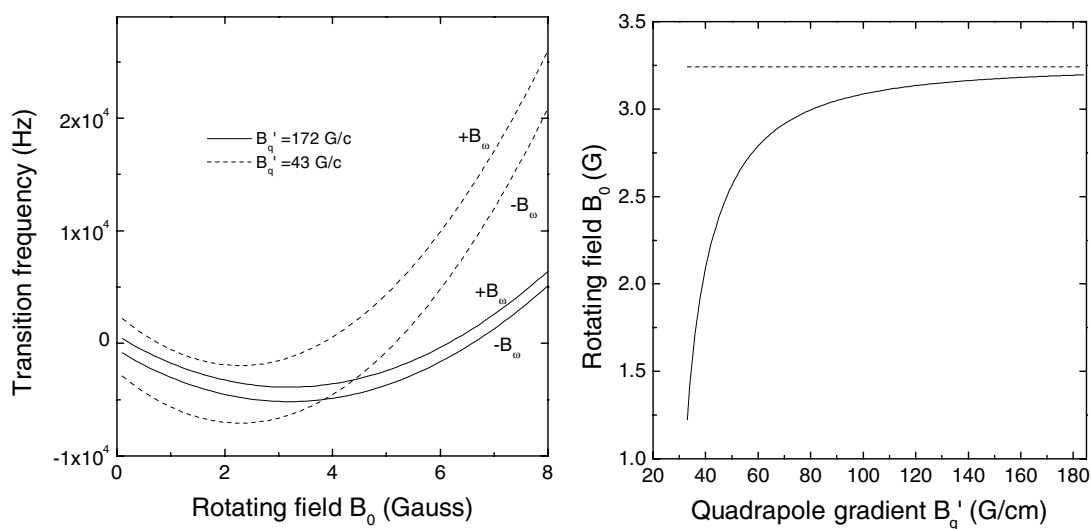


Figure 3.10: (a) The transition frequency as a function of the rotating field B_0 , similar to Fig. 3.2(b), but here the complete, time-dependent model is included. Each pair is for a different vertical gradient. Within each pair the effect of the rotating field is shown for the two directions of rotation $\pm B_\omega$. (b) The value of B_0 where the transition is insensitive to changes in field, plotted against B'_q . The dashed line is 3.241 G.

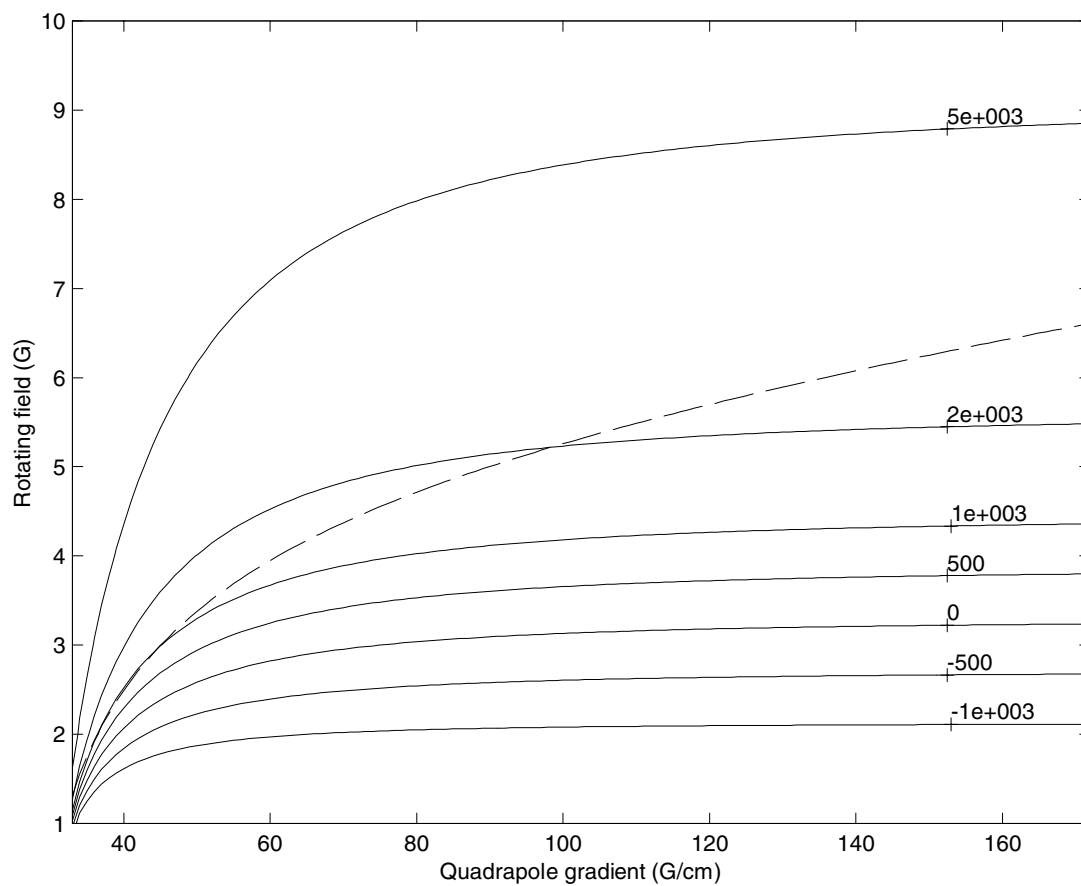


Figure 3.11: The contour plot shows the slope of the two-photon transition with respect to B_0 . Lines are labeled in Hz. The dotted line is the B_0 required for completely overlapping traps, for the frequency of field rotation of 1800 Hz.

3.4 Rabi frequency gradient across the condensate

The previous section dealt with the basic effects of the TOP trap and the higher order Zeeman structure on the two-photon transition. This section will specialize to a remarkably useful consequence of these effects; a gradient in the two-photon effective Rabi frequency Ω_{eff} across the condensate. As will be shown in Chapter 7, the gradient provides a way to manipulate the phase of a condensate spatially and temporally. There are essentially three different (although not independent) effects: trap offset, intermediate state detuning, and polarization of the two-photon drive.

3.4.1 Trap offset

The vertical offset between the equilibrium positions of the two states was given in Eq. 3.17 and Fig.3.9. This comes into Ω_{eff} through the detuning of the two-photon drive from resonance:

$$\Omega_{\text{eff}} = \sqrt{\Omega_0^2(z) + \Delta^2(z)} \quad (3.21)$$

where Ω_0 , the bare Rabi frequency from Eq. 3.1 and has no z dependence in this case, and

$$\begin{aligned} \Delta(z) &= \delta + \frac{1}{2} \frac{m}{\hbar} \omega^2 z^2 - \frac{1}{2} \frac{m}{\hbar} \omega^2 (z + z_{\text{offset}})^2 \\ &\rightarrow \delta + \frac{m}{\hbar} \omega^2 z_{\text{offset}} z. \end{aligned} \quad (3.22)$$

This equation for $\Delta(z)$ includes an overall detuning δ (a simple detuning of the drive from the resonance) and the detuning due to offset harmonic oscillator potentials. For strong field gradients the offset is simply $2B_\omega/B'_q$. The trap oscillation frequency ω is nearly the same for both states. In the limit that $\Omega_0 \ll \Delta(z)$ or $\delta \gg$ the detuning across the condensate, the effective Rabi frequency becomes simply $\Delta(z)$ and there is a linear gradient in Ω_{eff} along the vertical dimension.

This gradient can be from 0 (overlapping traps) to a few kHz over the extent of the condensate.

3.4.2 Intermediate-state detuning

The bare Rabi frequency Ω_0 from Eq. 3.1 may also be modified by changing the intermediate-state detuning Δ_{IM} as a function of vertical position (refer to Fig. 3.1). Since the $|2, 0\rangle$ state has no magnetic field dependence, and the $|2, 1\rangle$ and $|1, -1\rangle$ shift essentially together at $\sim \mu_b/(2h) \simeq 0.7$ MHz/G, the virtual intermediate-state will shift, locked with the $|2, 1\rangle$ and $|1, -1\rangle$ at 0.7 MHz/G. The gradient B' in which the condensate sits is where gravity is canceled, *i.e.* $B'\mu_b/2 = mg$ (higher order Zeeman terms are ignored). B' is approximately 30.5 G/cm for both $|2, 1\rangle$ and $|1, -1\rangle$. The total intermediate state detuning is then

$$\begin{aligned}\Delta_{IM} &= \Delta_{IM0} + \frac{\mu_b}{2h} B' z \\ &= \Delta_{IM0} + \frac{mg}{h} z \\ &= \Delta_{IM0} + 2140z \frac{\text{kHz}}{\mu\text{m}}\end{aligned}\tag{3.23}$$

where $z = 0$ is at the equilibrium position of the condensate, and Δ_{IM0} is the detuning of the microwave and rf from the $|2, 0\rangle$ where $z = 0$. The magnitude of this effect can be controlled by changing the size of the condensate (by changing ω), changing the relative strength of Ω_0 and the detuning, or by changing Δ_{IH} . The size of this effect is variable from a few Hz to kHz. A gradient in Ω_{eff} due to a gradient in Ω_0 is advantageous since the entire condensate is still in resonance, as opposed to a gradient in the detuning Δ in which the transfer between the two states also varies along z .

3.4.3 Drive polarization

The polarization of the two-photon drive can also be made to vary across the vertical direction. This occurs by changing the direction of an atom's quantization axis by varying the relative magnitude of the fields B_0 and B'_q . As the confining potential is lowered, the atoms sag further down due to gravity, experiencing a difference in the vertical magnetic field component. This alters the projection of the microwave and rf drives onto the quantization axis, changing the bare Rabi frequency for each drive in Eq. 3.1. Since the rf and microwave have the same polarization, this effect gets squared for the two-photon transition. Taking the first order term for the position of the atoms in the trap (Eq. 3.17), the bare Rabi frequency and its gradient for the full two-photon transition become respectively

$$\Omega_0 \rightarrow \Omega_0(1 - \eta^2) \quad (3.24)$$

$$\frac{\partial \Omega_0}{\partial z} = -2\Omega_0 \frac{B'_q}{B_0} \eta (1 - \eta^2)^{3/2}. \quad (3.25)$$

These are plotted in Fig. 3.12. Fig. 3.12a is a plot of the fractional change in Ω_0 at the center of the condensate as the quadrupole gradient is changed. It is interesting that this is independent of the rotating field B_0 . Fig. 3.12b is a plot of the fractional gradient in Ω_0 . In Fig. 3.12c, this gradient is multiplied by the Thomas-Fermi vertical width (full-width at zero) [53] of the condensate to show the fraction change in Ω_0 across the condensate. In general this effect accounts for only a few Hz across the cloud, but could be made ~ 100 Hz.

The previous analysis assumed that the polarization of the microwave and rf were along the rotating field's axis. This is nominally true, but interaction with the conducting coil forms and supports likely modifies these fields in an unknown way. As an estimate, I assume the field polarization angle to maximize the gradient of polarization across the cloud, which gives an increase by a factor of 2.4. This is the maximum increase, and only applies for a specific B'_q in Fig. 3.12,

which depends on the real angle of field polarization. For the case of the Rabi frequency gradient in Chapter 7, this maximum corresponds to ~ 18 Hz across the condensate.

3.5 Density shift

This shift is not a property of the magnetic trap as all the previous effects have been, but still provides a systematic in the two-photon transition frequency. Repulsive interactions between ^{87}Rb atoms in a BEC lead to an energy offset from the ground state of the harmonic oscillator. Since the strength of the interactions is different for different internal states, there can be a systematic shift in the transition frequency between the states which will depend on relative state populations. This is a small effect by the standards here, but well known in atomic clocks as the clock-shift, or pressure shift [98]. The difference in interaction energy between the states is [53]

$$E = 5\pi \frac{\hbar^2}{m} [(a_{11} \langle n_1 \rangle - a_{22} \langle n_2 \rangle) + a_{12} (\langle n_2 \rangle - \langle n_1 \rangle)]. \quad (3.26)$$

where $\langle n \rangle$ is the density-weighted average density in the Thomas-Fermi limit, and a_{ij} is the s -wave scattering length between states i and j . The first group of terms comes from the self-interaction energy and the second group from the mutual interaction between the two states. We are concerned with only the following values; $a_{11} = 107$, $a_{22} = 101$, and $a_{12} = 104$ in units of the Bohr radius $a_0 = 0.529 \times 10^{-8} \text{cm}$ [46]. In a usual Ramsey-type clock, the two states involved have equal superpositions during the time between the $\pi/2$ -pulses. For typical condensate densities of $5 \times 10^{13} \text{cm}^{-3}$, the shift is 30 Hz.

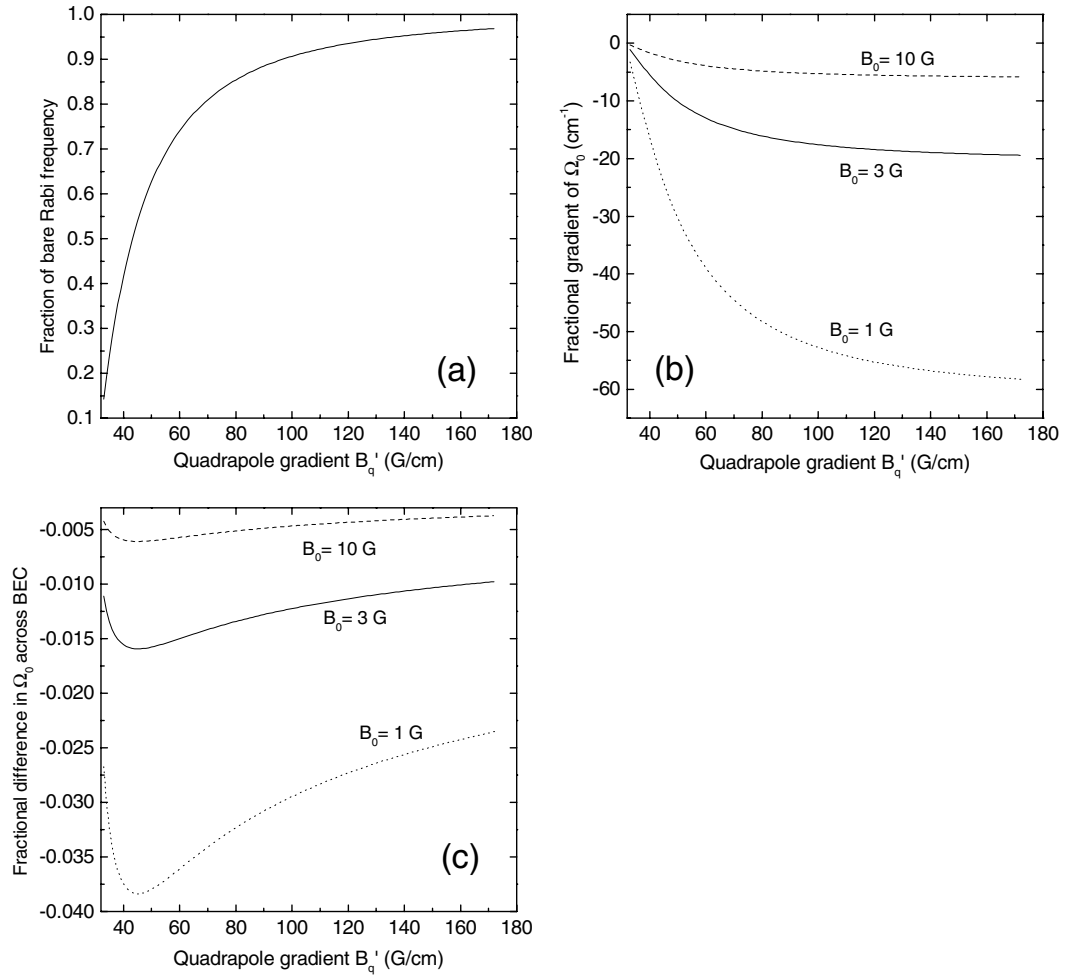


Figure 3.12: (a) The fractional change in bare Rabi frequency as a function of B'_q , due to a spatial gradient in polarization direction of the microwave and rf. (b) The fractional gradient in Ω_0 for three different values of the rotating field B_0 . (c) The fractional difference in bare Rabi frequency across the cloud due to a gradient in the two-photon drive polarization. Multiply this by Ω_0 to get the absolute difference in bare Rabi frequency across the condensate's diameter.

3.6 Tilted TOP

One last effect is introduced as a possible explanation for two effects common in two-state experiments; sidebands and radial symmetry breaking. A systematic study of sidebands on the transition profile has not been done, and the only real knowledge we have is that they are separated from the central carrier by the TOP rotation frequency ω_t . Radial symmetry breaking is observed as a separation of two-component condensates in a specific direction perpendicular to the trap's symmetry axis (see Fig. 3.8) as will be discussed later. A possible explanation is a tilt of the axis of $\vec{\omega}_t$ in Fig. 3.8 relative to the axis of the quadrupole coils. The resulting field from a tilt by angle θ in the \hat{x} direction is

$$|B_{\text{total}}(z)| = \left[\left(B_0 \cos \theta \cos(\omega_t t) + \frac{B'_q}{2} x \pm B_\omega \sin \theta \right)^2 + \left(B_0 \sin(\omega_t t) + \frac{B'_q}{2} y \right)^2 + \left(-B'_q z \pm B_\omega \cos \theta + B_0 \cos \theta \cos(\omega_t t) \right)^2 \right]^{\frac{1}{2}}. \quad (3.27)$$

Two effects are present here. First, since the condensate experiences a field component in the \hat{z} direction due to gravitational sag, the magnitude of the \hat{z} -component oscillates at the TOP frequency ω_t (third term). It causes a modulation of the transition frequency and thus sidebands. This can be thought of as a modulated drive; $\omega(t) = \omega_c + \Delta\omega \cos \omega_m t$ where ω_c and ω_m are the carrier and modulation frequencies, and $\Delta\omega$ is the amount of frequency modulation. To estimate the size of this effect, I start by estimating the on resonance Rabi frequency of the sideband Ω_{sb} , as ~ 0.4 of the Rabi frequency of the carrier Ω_c (determined from fig. 3.5). In the region of wide-band phase modulation the electric field can be written as

$$E(t) = A_c J_0(\beta) \cos \omega_c t - A_c J_1(\beta) (\cos(\omega_c + \omega_m)t - \cos(\omega_c - \omega_m)t) + \dots \quad (3.28)$$

where A_c is the amplitude of the carrier for zero modulation, J_0 and J_1 are Bessel functions, and $\beta \equiv \Delta\omega/\omega_m$ is the modulation index. The ratio of Rabi frequencies

is then just that of the amplitudes squared $(J_1(\beta)/J_0(\beta))^2$ which implies $\beta \simeq 1$.

It is now necessary to estimate how big the TOP tilt must be to produce this size of modulation of the two-photon transition. To produce a modulation index of 1, $\Delta\omega \simeq \omega_t = 1800$ kHz. This amount of modulation gives an amount of magnetic field modulation through the derivative of Eq. 3.5, which is 100 Hz/G for $B_{\text{total}} = 3.5$ G. I take instead the very conservative limit of 500 Hz/G, implying a field modulation of 3.6 G which is larger than the total field. Obviously this cannot be the cause of the sidebands.

For completeness, I estimate the effect of a more reasonable tilt. The peak to peak amplitude of oscillation of the total magnetic field for small tilts θ , from Eq. 3.27 is

$$\Delta B_{pp} \simeq 2\eta(B'_q)B_0\theta. \quad (3.29)$$

A tilt of 5° gives $\Delta B \simeq 0.3$ G out of $\simeq 3.5$ G total field. The slope is again taken to be 500 Hz/G (five times larger than the actual slope at $B_{\text{total}} = 3.5$ G) which means a frequency modulation of $\Delta\omega = 150$ Hz and a modulation index $\beta = \Delta\omega/\omega_{\text{top}} = 150/1800$.

Unfortunately a detailed study of sidebands has not been done, even though they are frequently an annoying presence. There are many features which have yet to be explained: Sidebands are present even for a dropped atom cloud ($B'_q = 0$, $B_\omega \neq 0$), implying the trap is not the cause (although an external field could take the place of the vertical field from the quadrupole); sidebands move and even switch sides about the carrier for different turn on times of the two-photon drive with respect to the rotating TOP field. This was true even when the two-photon pulse length is comparable to the TOP rotation period (It should be stressed that this latter observation was made with a different placement of the microwave waveguide, and has not been investigated for the current placement shown in Fig.

3.3).

A second effect of the tilt is a component of the imaginary field B_ω along the \hat{x} direction (first term), thereby giving an offset similar to that discussed previously in the \hat{z} direction. In this case however, gravity is perpendicular to the offset and so the higher-order Zeeman shifts cannot be used to cancel the offset as in Fig. 3.9. The magnitude of the offset is $4B_\omega \sin \theta / B'_q$. For $\theta = 5$ degrees, a vertical gradient of $B'_q = 122$ G/cm (17 Hz radial frequency), and a TOP rotation of 1800 kHz, this comes out to $\sim 0.08 \mu\text{m}$. See Fig. 5.4 for the data corresponding to this trap, showing the radial offset. To put this offset in perspective, it is compared with the vertical separation in a trap with vertical gradient of 129 G/cm, vertical frequency of 62 Hz, and an offset of $0.4 \mu\text{m}$, seen in Fig. 5.5. In that case the time for appreciable separation was 10 ms. In the case of radial separation in Fig. 5.4 the radial separation time was about 100 ms. A rough scaling of the separation time in each case by the offset and the relevant trap frequency gives $(17 \times .08 \times 100) = 136$ and $(62 \times .4 \times 10) = 248$ shows a factor of two difference for a 5 degree tilt. A 10 degree tilt is somewhat unlikely, but the estimate shows the effect is in the right neighborhood.